Accelerate Synthesis of Metal-Organic Frameworks by a Robotic Platform and Bayesian Optimization

Yunchao Xie[1], Chi Zhang[1], Heng Deng[1], Bujingda Zheng[1], Jheng-Wun Su[3], Kenyon Shutt[1], and Jian Lin[1,2*]

[1]Department of Mechanical and Aerospace Engineering,
[2]Department of Electrical Engineering and Computer Science, University of Missouri, Columbia, Missouri 65211, USA
[3]Department of Physics and Engineering, Slippery Rock University, Slippery Rock, Pennsylvania 16057, USA
[*]E-mail: LinJian@missouri.edu (J. L.)

Abstract

Synthesis of materials with desired structures, e.g. metal-organic frameworks (MOFs), involves optimization of highly complex chemical and reaction spaces due to multiple choices of chemical elements and reaction parameters/routes. Traditionally, realizing such an aim requires rapid screening of these nonlinear spaces by experimental conduction by human intuition, which is quite inefficient and may cause errors or bias. In this work, we report a platform that integrates a synthesis robot with a Bayesian optimization (BO) algorithm to accelerate the synthesis of MOFs. The robotic platform consists of an automatic direct laser writing apparatus, precursors injecting and Joule-heating components. It can automate the synthesis upon fed reaction parameters which are recommended by the BO algorithm. Without any prior knowledge, this integrated platform continuously improves the crystallinity of ZIF-67, a demo MOF employed in this study, as the operation iterations increase. This work represents a methodology enabled by a data-driven synthesis robot which achieves the goal of material synthesis with targeted structures, thus greatly shortening the reaction time and reducing energy consuming. It can be easily generalized to other material systems, thus paving a new route to autonomous discovery of a variety of materials in a cost-effective way in future.

Keywords: Bayesian optimization, metal-organic frameworks, robotic platform, automation, crystallinity

Introduction

Metal-organic frameworks (MOFs), built from metal ions and organic linkers, have emerged as promising materials for gas adsorption/separation,[1-3] sensors,[4-5] catalysis,[6-7] and drug delivery[8-9] due to their high porosity and chemical tunability.[10-11] Until now, several methodologies including hydro/solvothermal, sonochemical, microfluidic, chemical vapor deposition, and mechanochemical reactions, have been developed towards synthesis of MOFs.[12-16] Crystallinity of MOFs can significantly impact the material properties, while realization of high crystallinity usually involves multiple choices of chemical elements and reaction parameters/routes.[17-20] The methods used in the reported works require long synthesis durations spanning from hours to days, making rapid screening of the chemical and reaction spaces almost unrealistic. In addition, in a traditional human centered process, experiments are designed *via* human intuition and performed by human who is error-prone, thus resulting in research outcomes with large variances.

High-throughput experimentation (HTE) performed by robotic platforms has emerged as an enabling technology to accelerate material development.[12, 21-24] Yaghi's group reported HTE of zeolitic imidazolate frameworks (ZIFs) enabled by commercial synthetic apparatus including robotic dispensing and handling hardware, and successfully isolated 25 ZIFs from 9600 reactions.[12] Greenaway *et al*. implemented commercial synthesizer platform for high-throughput screening of 78 building block combinations, which led to synthesis of 33 organic cages.[21] Furthermore, integrating optimization algorithms such as curious algorithm (CA),[25] genetic algorithm (GA)[26-28] and Bayesian optimization (BO)[29-31] with HTE holds the promise to greatly minimize the total number of required experiments, thus greatly accelerating the whole workflow by an order of magnitude. Apart from predicting the physical and chemical properties,[32] establishing the structure-property relationship,[33-34] and guiding materials synthesis,[35] data driven

algorithms by artificial intelligence/machine learning (AI/ML) such as support vector machine (SVM)[36] and random forest (RF)[37-38] have also been deeply involved in the experimental optimization processes.[39-46] Grizou and his colleagues reported a CA-guided chemical robot for efficiently exploring complex chemical spaces.[25] Pavel and his colleagues built an autonomous research system (ARES) *via* integrating a planner of RF/GA with an automated growth reactor for automatically optimizing the growth parameters of carbon nanotubes.[47] Macleod and co-workers integrated ChemOS, which uses the *Phoneics* global BO algorithm, with customized modular robot platform to autonomously optimize the hole mobility of thin film.[29] Gongora *et al*. developed a Bayesian experimental autonomous researcher (BEAR) for autonomously optimizing the mechanical properties of 3D printed parts.[30] Although integration of these optimization algorithms with HTE is a powerful tool for accelerating materials development, its applications in materials development are still in its infancy and being continuously developed. For instance, development of an autonomous robot for rapid MOF synthesis has yet been demonstrated. To realize this goal, a paramount requirement is to develop a processing method that can rapidly synthesize MOFs.

Recently, our group demonstrated two new methodologies, i.e., Joule and microwave-heating to rapidly synthesize zeolitic imidazolate frameworks (ZIFs).[48] During Joule heating (JH), Laser-induced graphene (LIG) was heat up to drive the conversion of precursors to ZIF-67 with well-controlled morphology and crystallinity. The JH methodology showed an obvious reduction in reaction durations, energy consumption and manufacturing costs. However, two limitations still exist by this approach. First, the whole experimental procedure is still manually conducted, which makes the material synthesis fall behind the pace of material discovery demanded in the era of automation. Second, lack of an optimization strategy results in limited exploration of chemical/reaction spaces towards synthesizing the optimized candidates.

Herein, we demonstrate a robotic platform combined with a BO algorithm for rapidly optimizing the synthesis variables to obtain ZIF-67 with improved crystallinity. The robotic platform consisted of four main components, i.e., the motion, lasing, injecting, and JH systems, for automating the synthesis of ZIF-67. The crystallinity of ZIF-67 was indeed improved with the increase of the synthesis iterations recommended by the BO algorithm. Contribution of our work to the field includes the following four aspects. First, development of a robotic platform enables the automated synthesis of ZIF-67. Such a robotic platform can be directly used for exploration of other MOFs. In future, a roll-to-roll technique can be integrated into the robotic platform for continuous manufacturing. Second, the automated synthesis of ZIF-67 enabled by the robotic platform led to shortened reaction time, reduced reagent consumption, and minimized human interference. Third, the BO algorithm recommends the optimized chemical compositions and reaction parameters to the robotic platform to synthesize ZIF-67 with continuously improved crystallinity. Fourth, the established process-property relationship helps to understand the reaction mechanism, which paves a new route to future design of materials with superior properties. Future work can be done by further integrating *in-situ* characterization instruments such as Raman, FTIR, and UV-vis spectrophotometers, automatic data analysis, and high-throughput electrochemical tests for the autonomous closed-loop materials development.

Results and Discussion

Previously, we reported the rapid synthesis of ZIF-67 *via* Joule-heating (JH) by using laser-induced graphene (LIG) as the microreactors.[48] The work showed two limitations, i.e., manual operation and lack of optimization of experiment. To solve the former limitation, herein, we designed and built a robotic experimental platform to perform the JH experiments in an automated

way. To solve the latter one, a BO algorithm was developed and integrated with the robotic platform for efficiently finding the optimized variables for rapid synthesis of ZIF-67 with improved crystallinity. The scheme illustrated in Figure 1 shows the synthesis and optimization workflow enabled by the developed robotic platform and the BO algorithm.

First, the search space was determined by two chemical compositions, a molar ratio of Co ions to 2-methylimidazole (MeIM) and a total volume of precursors, and two processing parameters, an applied DC voltage and reaction time. Then, combination of these four variables was sampled from the search space using the BO algorithm. These four variables were coded in a G-code format and sent to the robotic platform for automatically synthesizing ZIF-67. The crystallinity of ZIF-67 was determined by measuring the full-width at half maximum (FWHM) of X-ray diffraction (XRD) patterns. The value of FWHM was fed as the optimization objective into the BO algorithm. Finally, the BO algorithm recommended a new set of the synthesis variables in the search space that were expected to synthesize ZIF-67 with increased crystallinity.

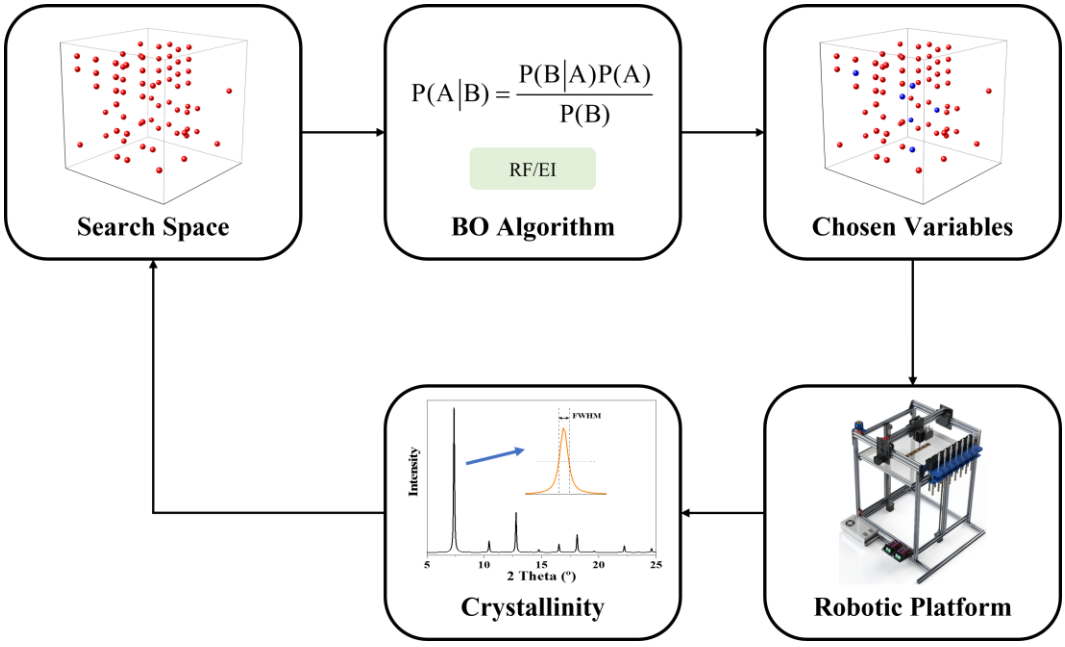

Figure 1. Schematic showing a process of synthesizing MOFs with improved crystallinity *via* integration of a robotic platform with BO algorithm.

Figure 2A and 2B shows a 3D rendering and a photograph of the robotic platform featuring four main components, i.e., the motion, lasing, injecting and Joule heating systems. The detailed bill of materials (BOM) for each component can be found in Table S1. The total cost of these parts for the robotic platform was ~$830. The moving system or so-called Gantry XYZ (Figure S1) was designed based on computer numerical control (CNC)[25, 49] and its mobility was controlled using a technology originally coded for an open-source "RepRap" 3D printer. The injecting system consists of two parts: a syringe pump (Figure S2) and a dispending needle (Figure S3). The syringe pump, which was modified according to the literature,[25] consists of 3D printed mounts, plastic syringe, check-valve, Luer-lock adapters, and stepper motor. Each syringe pump was calibrated, and the testing results were shown in Table S2. The precursors with specific molar ratios were in advance loaded into the syringes after preparation. The dispending needle was fixed to Gantry X and consists of a 3D-printed mount, a Luer-lock needle, a Y adapter, and a Female Luer-to 1/4"-28 UNF Female adapter. A polytetrafluoroethylene (PTFE) tube was cut into 100 cm length for connection of the syringe pump and the dispensing needle. The lasing system, consisting of a 5.5 W blue laser, was used to fabricate LIG microreactors on a polyimide (PI) thin film. Joule heating system was designed to provide DC voltage for rapidly heating up the LIG microreactor. A Rotary switch (Figure S4) was used to switch on/off the DC voltage. An Arduino RAMPS board (Figure S5) is assembly of an Arduino Mega 2560 R3 and a RAMPS 1.6 plus board. It was used to receive and execute the G-Code commands.

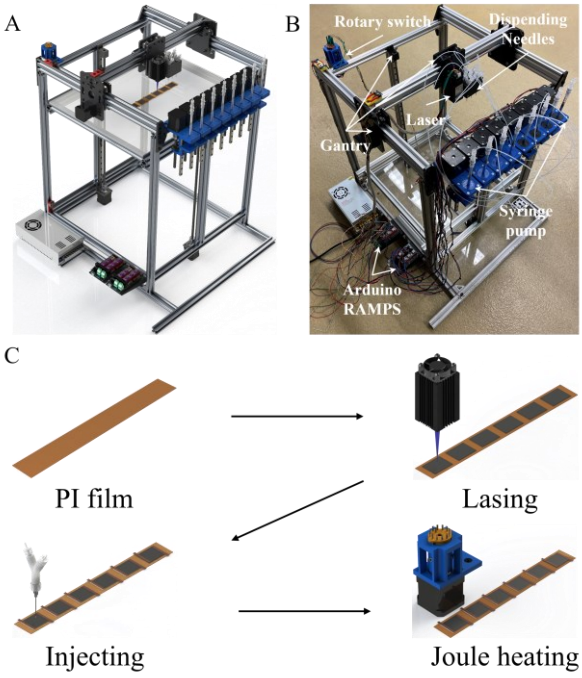

Figure 2. (A) 3D rendering and (B) photograph of a home-made robotic platform. (C) Flow chart of automated synthesis process procedure of ZIF-67 using the robotic platforms.

Detailed wiring of each component to two Arduino RAMPS boards can be found in Figure S6. The Gantry XYZ, rotary switches, and the blue laser were connected to the X, Y, Z, E0 and D9 interface ports of the first Arduino RAMPS board, respectively. Four syringe pump couples and the JH cable were connected to the X, Y, Z, E0 and D9 interface ports of the second Arduino RAMPS board, respectively. The detailed control logic can be found on Figure S8. Marlin firmware was modified and uploaded to the Arduino Mega 2560 board. All the linear movement of these components such as Gantry XYZ and the syringe pumps can be controlled by G1 command with the given distance and federate. For example, G1 X10 F1000 means moving the distance of 10 mm on the X axis with the feedrate of 1000 mm/min. Turning on/off the blue laser and JH was controlled by the M106 command with given numbers. For instance, M106 S203 outputs DC of 10 V from the D9 port, while G4 S300 keeps the output for 5 min. The detailed

correlation between the DC voltage from the D9 port and G-code command M106 can be found in Figure S7.

Figure 2C depicts a typical procedure for the automatic synthesis of ZIF-67 *via* the JH technique using the robotic platform (Supplementary Video 1). First, the LIG microreactors were prepared on a PI film using laser induction with an optimized laser power and a scan rate.[50] Then, the electrodes of LIG were cast with silver paints and extended with conductive copper tapes to the alligator clips affiliated with the rotary switch. After that, a predetermined volume of the precursors containing Co^{2+} and MeIM was injected to the surface of LIG microreactor *via* the dispensing needles from the syringe pump couples. Then, the DC voltage was applied to the electrodes of the LIG microreactors for controlled durations, during which the heating generated by the LIG microreactors converted the precursors into ZIF-67.

To improve the crystallinity of the ZIF-67, a BO algorithm[51] was implemented for efficiently sampling the synthesis variables from the search space. Description of BO can be found in supporting information. BO has shown considerable promise in materials discovery for navigating Quantitative Structure-Pharmacokinetics Relationship (QSPR) space, property prediction, and synthesis optimization.[26, 51-55] Herein, the search space to be explored consists of four variables: the ratios of the metal ions to the organic linkers, the volumes of the precursors, the applied DC voltages, and the Joule heating durations (Table S3). The optimization objective was the crystallinity of the synthesized ZIF-67. First, four variables (molar ratio, volume, DC voltage and JH durations) recommended by the BO algorithm were programmed in G-code command. Then, the G-code was sent to two Arduino RAMPS boards for driving the smooth operation of each component. The as-synthesized ZIF-67 was characterized using XRD and its crystallinity was determined by calculating the FWHM (Figure S9). FWHM can be a straightforward indicator of

materials' crystallinity.[26] It can be derived from the Scherrer equation: $D = K\gamma/(\beta\cos\theta)$, where K is a dimensionless shape factor, γ refers to the wavelength of X-ray, β refers to the FWHM of XRD pattern, and θ refers to the Bragg angle.[56] First, FWHM can be obtained *via* fitting the peaks using Gaussian function according to the following formula $FWHM = 2\sqrt{2\ln 2}\sigma$, where σ refer to the standard deviation. Then, the FWHM at 2θ of 7.36º, 10.42º, 14.76º, 16.52º, 18.10º was averaged. Finally, the ratio of the averaged FWHM of experimental to theoretical XRD pattern was reported as the crystallinity indicator. The calculated crystallinity values were the output of the BO algorithm. Initially, the BO algorithm randomly selected the four synthesis variables. The BO algorithm was then updated based on the outcome of the measured crystallinity. Based on the result from the previous iterations, it recommended the synthesis variables for the next cycle of experiment. Finally, the crystallinity was improved as the iteration increased (detailed iterations can be found in Table S4).

BO with the random forest (BO-RF) as a surrogate model was implemented to optimize the crystallinity of ZIF-67. BO was selected based on two considerations.[57] First, BO is simple to implement since it requires less hyperparameters tuning. Second, BO is excellent in processing sparse datasets. Within a smaller number of initial datasets and less iterations steps, BO can quickly find the optimal parameters than a genetic algorithm.[58] As for the surrogate model, RF, instead of the Gaussian process, was chosen since the search space contains categorical and continuous variables.[51] BO-RF can maximize the objective function which is then evaluated by an acquisition function (expected improvement, EI) *via* quantifying the utility of candidates (Figure 3A). As shown in Figure 3B, FWHM of representative peaks in the XRD spectra of four ZIF-67 samples synthesized with the reaction parameters recommended by BO-RF decreased as the increased iterations, suggesting the improved crystallinity. Figure 3C exhibited the evolution of crystallinity

of ZIF-67. It can be seen that variance of FWHM of all ZIF samples synthesized in the different iterations converges to higher values, indicating that the decreased quality variances (Figure 3B). In addition, the mean value over the samples synthesized from recommendations of BO is calculated to be 0.67, which is higher than that of random optimization (0.47). This result further confirmed the improvement of BO over the random optimization.

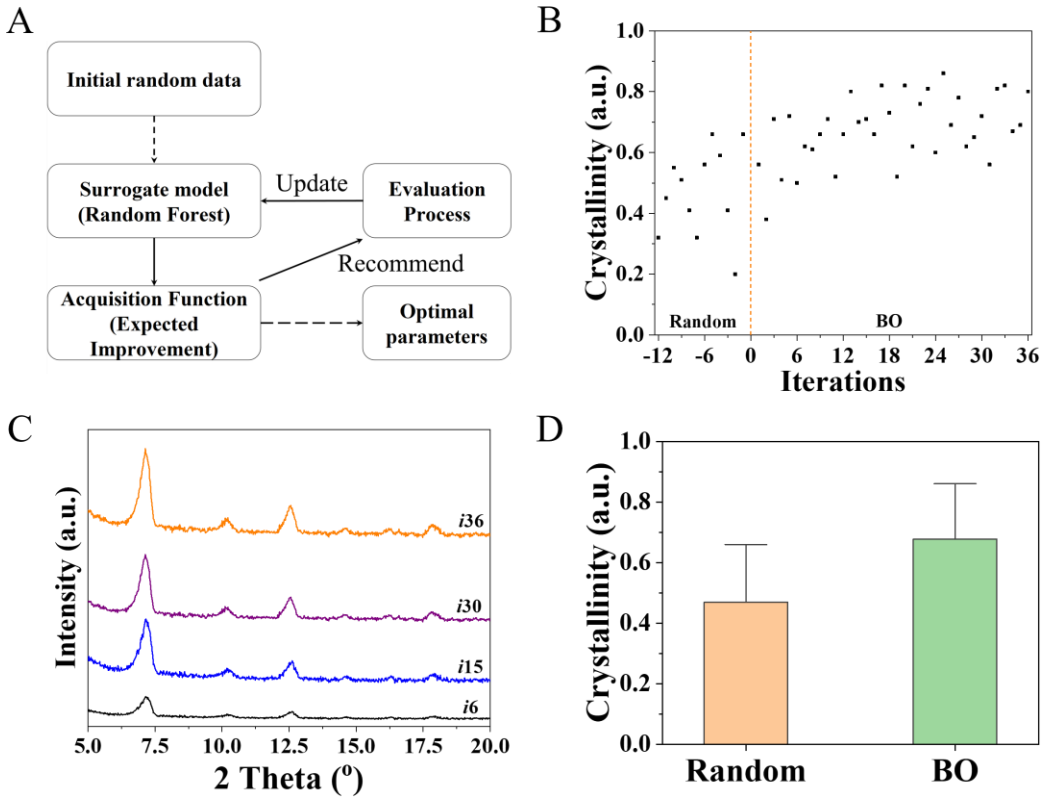

Figure 3. (A) Flowchart showing the BO process. (B) XRD patterns of four representative ZIF-67 synthesized with the reaction parameters recommended at different iterations. (C) Evolution of crystallinity *vs*. the generations of BO. (D) Bar chart showing statistics of the achieved crystallinity over the random and BO optimization processes. The error bar in (D) indicates the standard deviation of the data obtained from (C).

The plots of crystallinity dependent on the four variables (Figure 4A and 4B, and their projection views can be found in Figure S10) showed that a higher crystallinity appears at the synthesis variables of smaller molar ratios, larger volumes of precursors and higher DC voltages while heating durations had the marginal contribution to the improvement of the crystallinity.

Figure 4C-4E show the partial dependence (PD) of marginal relationship between the synthesis parameters and crystallinity. Due to its categorical property, real value of the molar ratio was shown in Figure 4F. The PD plots reveal the margin relationship between the continuous parameters in search space and the optimal crystallinity. The surrogate model (RF) was first trained on the available datapoints, then used to predict the EI value. From Figure 4C-4E, one can find that the crystallinity gradually increased as the increase of volume and voltage, and first increased then gradually decreased as the increase of time. This trend is similar as that of molar ratio (Figure 4F). It is obvious that a higher molar ratio leads to a higher crystallinity.

To further illustrate the correlation of the crystallinity with the four variables, we also trained a multilayer perceptron algorithm (MLP) from all the experimental data. Figure S11A and 11B showed the histogram of the crystallinity and heatmap of the four variables. From Figure S11C and S11D, we can see that a higher crystallinity appears under the reaction conditions with a smaller molar ratio, a higher precursors volume, a higher DC voltage, and lower reaction time. This result is in good agreement with the previous findings shown in Figure 4. These results validate that BO-RF can be applied to optimize experiments so that the required number of background experiments performed on a robotic platform can be reduced. The demonstrated robotic platform showed impressive capability of reaching the optimal results within relatively small iterations. Considering that the experiments performed by the robot can minimize human bias and intervention, this platform would afford a promising paradigm for future material development.

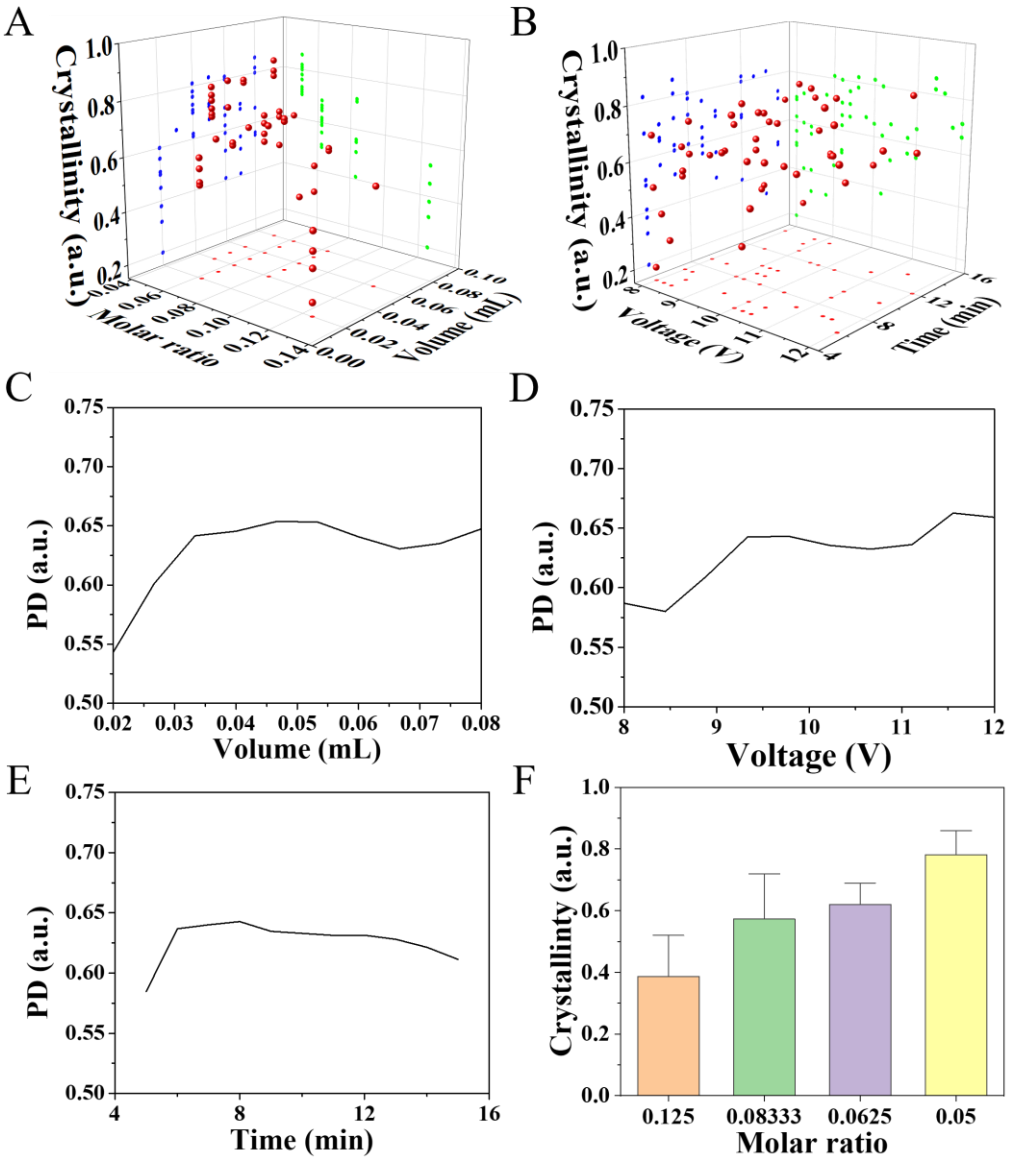

Figure 4. Plots of crystallinity on (A) the molar ratio and volume and (B) the DC voltage and reaction durations. Partial dependence plots of crystallinity over (C) volume, (D) voltage, and (E) Time. (F) Box chart of crystallinity over molar ratio.

Conclusion

In summary, in this work we reported integration of a robotic synthesis platform with the BO optimization algorithm for rapid synthesis of MOFs with improved crystallinity. An automatic synthesis robot was designed and constructed to realize the goal. In addition, the applied BO-RF

could successfully optimize the crystallinity of ZIF-67 within limited iterations. The partial dependencies showed that the molar ratio, precursors volume, and DC voltage played much more important role in improving the crystallinity than the reaction duration. This methodology not only greatly shortens the reaction time, reduces energy consumption and toxic wastes, but also provides a general platform for synthesis, optimization and discovery of new materials, thus paving a new avenue to other metal-organic complexes where the target materials are built from metal ions and organic linkers. There are still several limitations including the manual measurement and analysis of XRD data, batch-to-batch manufacturing and non-closed-loop optimization, which restricts the further development of robotic platform. In future, an autonomous platform that incorporates *in-situ* characterization techniques, automatic data analysis, and self-optimization algorithms will be developed to greatly accelerate the rate of materials processing.

Supporting Information

Experimental section; 3D rendering of Gantry X (A), Y (B), and Z (C); 3D rendering (A, B, C and D) and photograph (E) of home-made syringe pump; 3D rendering (A, B, C and D) and photograph (E) of dispending needles; 3D rendering (A, B, C and D) and photograph (E) of rotary switch; 3D rendering (A, B, C, D and E) and photograph (F) of Arduino RAMPS; Detailed wiring of each component to two Arduino RAMPS boards; Correlation between the G-code command (M106 S) and the output DC voltage from D9 port of RAMPS 1.6 plus board; A flowchart showing the control and the command logic; A theoretical XRD pattern of ZIF-67; Crystallinity *vs*. (A) molar ration, (B) volume, (C) voltage and (D) time over BO; (A) Histogram of crystallinity, (B) Heatmap of four variables, Contour maps of crystallinity as a function of ratio and volume (C), and voltage and time (D); Bill of Materials (BOM) and cost for building the robotic platform; Calibration of

syringe pump; Synthesis variables used in the experiments; Iterations of the crystallinity of ZIF-67 over BO; Hyperparameters of multilayer perceptron.

Acknowledgement

This work was financially supported by grants from National Science Foundation (award number: 1825352 and 1933861), United States Department of Energy National Energy Technology Laboratory (award number: DE-FE0031645), and Sony Research Award Program 2019.

Code availability.

The corresponding codes can be available at https://github.com/linresearchgroup/Robot_MOF.

Declaration of interests

The authors declare no competing interests.

References

(1) Murray, L. J.; Dincă, M.; Long, J. R. Hydrogen storage in metal–organic frameworks. *Chem. Soc. Rev.* **2009,** *38*, 1294-1314.
(2) Li, J.-R.; Kuppler, R. J.; Zhou, H.-C. Selective gas adsorption and separation in metal–organic frameworks. *Chem. Soc. Rev.* **2009,** *38*, 1477-1504.
(3) Li, J.-R.; Sculley, J.; Zhou, H.-C. Metal–Organic Frameworks for Separations. *Chem. Rev.* **2012,** *112*, 869-932.
(4) Li, H.-Y.; Zhao, S.-N.; Zang, S.-Q.; Li, J. Functional metal–organic frameworks as effective sensors of gases and volatile compounds. *Chem. Soc. Rev.* **2020,** *49*, 6364-6401.
(5) Koo, W.-T.; Jang, J.-S.; Kim, I.-D. Metal-Organic Frameworks for Chemiresistive Sensors. *Chem* **2019,** *5*, 1938-1963.
(6) Pascanu, V.; González Miera, G.; Inge, A. K.; Martín-Matute, B. Metal–Organic Frameworks as Catalysts for Organic Synthesis: A Critical Perspective. *J. Am. Chem. Soc.* **2019,** *141*, 7223-7234.
(7) Wang, T.; Gao, L.; Hou, J.; Herou, S. J. A.; Griffiths, J. T.; Li, W.; Dong, J.; Gao, S.; Titirici, M.-M.; Kumar, R. V.; Cheetham, A. K.; Bao, X.; Fu, Q.; Smoukov, S. K. Rational approach to guest confinement inside MOF cavities for low-temperature catalysis. *Nat. Commun.* **2019,** *10*, 1340.
(8) Wu, M.-X.; Yang, Y.-W. Metal–Organic Framework (MOF)-Based Drug/Cargo Delivery and Cancer Therapy. *Adv. Mater.* **2017,** *29*, 1606134.

(9) Suresh, K.; Matzger, A. J. Enhanced Drug Delivery by Dissolution of Amorphous Drug Encapsulated in a Water Unstable Metal–Organic Framework (MOF). *Angew. Chem. Int. Ed.* **2019,** *58*, 16790-16794.
(10) Zhou, H.-C.; Long, J. R.; Yaghi, O. M. Introduction to Metal–Organic Frameworks. *Chem. Rev.* **2012,** *112*, 673-674.
(11) Wang, Q.; Astruc, D. State of the Art and Prospects in Metal–Organic Framework (MOF)-Based and MOF-Derived Nanocatalysis. *Chem. Rev.* **2020,** *120*, 1438-1511.
(12) Banerjee, R.; Phan, A.; Wang, B.; Knobler, C.; Furukawa, H.; O'Keeffe, M.; Yaghi, O. M. High-Throughput Synthesis of Zeolitic Imidazolate Frameworks and Application to CO_2 Capture. *Science* **2008,** *319*, 939-943.
(13) Chen, Y.; Ji, S.; Wang, Y.; Dong, J.; Chen, W.; Li, Z.; Shen, R.; Zheng, L.; Zhuang, Z.; Wang, D.; Li, Y. Isolated Single Iron Atoms Anchored on N‐Doped Porous Carbon as an Efficient Electrocatalyst for the Oxygen Reduction Reaction. *Angew. Chem. Int. Ed.* **2017,** *56*, 6937-6941.
(14) Cho, H.-Y.; Kim, J.; Kim, S.-N.; Ahn, W.-S. High yield 1-L scale synthesis of ZIF-8 via a sonochemical route. *Microporous Mesoporous Mater.* **2013,** *169*, 180-184.
(15) Brown, A. J.; Brunelli, N. A.; Eum, K.; Rashidi, F.; Johnson, J. R.; Koros, W. J.; Jones, C. W.; Nair, S. Interfacial microfluidic processing of metal-organic framework hollow fiber membranes. *Science* **2014,** *345*, 72-75.
(16) Beldon, P. J.; Fábián, L.; Stein, R. S.; Thirumurugan, A.; Cheetham, A. K.; Friščić, T. Rapid Room-Temperature Synthesis of Zeolitic Imidazolate Frameworks by Using Mechanochemistry. *Angew. Chem. Int. Ed.* **2010,** *49*, 9640-9643.
(17) Lee, H. J.; We, J.; Kim, J. O.; Kim, D.; Cha, W.; Lee, E.; Sohn, J.; Oh, M. Morphological and Structural Evolutions of Metal–Organic Framework Particles from Amorphous Spheres to Crystalline Hexagonal Rods. *Angew. Chem. Int. Ed.* **2015,** *54*, 10564-10568.
(18) Ji, H.; Lee, S.; Park, J.; Kim, T.; Choi, S.; Oh, M. Improvement in Crystallinity and Porosity of Poorly Crystalline Metal–Organic Frameworks (MOFs) through Their Induced Growth on a Well-Crystalline MOF Template. *Inorg. Chem.* **2018,** *57*, 9048-9054.
(19) Choi, J.-S.; Son, W.-J.; Kim, J.; Ahn, W.-S. Metal–organic framework MOF-5 prepared by microwave heating: Factors to be considered. *Microporous Mesoporous Mater.* **2008,** *116*, 727-731.
(20) Farha, O. K.; Spokoyny, A. M.; Mulfort, K. L.; Galli, S.; Hupp, J. T.; Mirkin, C. A. Gas-Sorption Properties of Cobalt(II)–Carborane-Based Coordination Polymers as a Function of Morphology. *Small* **2009,** *5*, 1727-1731.
(21) Greenaway, R. L.; Santolini, V.; Bennison, M. J.; Alston, B. M.; Pugh, C. J.; Little, M. A.; Miklitz, M.; Eden-Rump, E. G. B.; Clowes, R.; Shakil, A.; Cuthbertson, H. J.; Armstrong, H.; Briggs, M. E.; Jelfs, K. E.; Cooper, A. I. High-throughput discovery of organic cages and catenanes using computational screening fused with robotic synthesis. *Nat. Commun.* **2018,** *9*, 2849.
(22) Palomba, J. M.; Credille, C. V.; Kalaj, M.; DeCoste, J. B.; Peterson, G. W.; Tovar, T. M.; Cohen, S. M. High-throughput screening of solid-state catalysts for nerve agent degradation. *Chem. Commun.* **2018,** *54*, 5768-5771.
(23) Daponte, J. A.; Guo, Y.; Ruck, R. T.; Hein, J. E. Using an Automated Monitoring Platform for Investigations of Biphasic Reactions. *ACS Catal.* **2019,** *9*, 11484-11491.
(24) Curtarolo, S.; Hart, G. L. W.; Nardelli, M. B.; Mingo, N.; Sanvito, S.; Levy, O. The high-throughput highway to computational materials design. *Nat. Mater.* **2013,** *12*, 191-201.
(25) Grizou, J.; Points, L. J.; Sharma, A.; Cronin, L. A curious formulation robot enables the discovery of a novel protocell behavior. *Sci. Adv.* **2020,** *6*, eaay4237.
(26) Moosavi, S. M.; Chidambaram, A.; Talirz, L.; Haranczyk, M.; Stylianou, K. C.; Smit, B. Capturing chemical intuition in synthesis of metal-organic frameworks. *Nat. Commun.* **2019,** *10*, 539.
(27) Kirman, J.; Johnston, A.; Kuntz, D. A.; Askerka, M.; Gao, Y.; Todorović, P.; Ma, D.; Prive, G. G.; Sargent, E. H. Machine-learning-accelerated perovskite crystallization. *Matter* **2020,** *2*, 938-947.
(28) Salley, D.; Keenan, G.; Grizou, J.; Sharma, A.; Martín, S.; Cronin, L. A nanomaterials discovery robot for the Darwinian evolution of shape programmable gold nanoparticles. *Nat. Commun.* **2020,** *11*, 1-7.

(29) MacLeod, B. P.; Parlane, F. G. L.; Morrissey, T. D.; Häse, F.; Roch, L. M.; Dettelbach, K. E.; Moreira, R.; Yunker, L. P. E.; Rooney, M. B.; Deeth, J. R.; Lai, V.; Ng, G. J.; Situ, H.; Zhang, R. H.; Elliott, M. S.; Haley, T. H.; Dvorak, D. J.; Aspuru-Guzik, A.; Hein, J. E.; Berlinguette, C. P. Self-driving laboratory for accelerated discovery of thin-film materials. *Sci. Adv.* **2020,** *6*, eaaz8867.
(30) Gongora, A. E.; Xu, B.; Perry, W.; Okoye, C.; Riley, P.; Reyes, K. G.; Morgan, E. F.; Brown, K. A. A Bayesian experimental autonomous researcher for mechanical design. *Sci. Adv.* **2020,** *6*, eaaz1708.
(31) Langner, S.; Häse, F.; Perea, J. D.; Stubhan, T.; Hauch, J.; Roch, L. M.; Heumueller, T.; Aspuru-Guzik, A.; Brabec, C. J. Beyond Ternary OPV: High-Throughput Experimentation and Self-Driving Laboratories Optimize Multicomponent Systems. *Adv. Mater.* **2020,** *32*, 1907801.
(32) Ward, L.; Agrawal, A.; Choudhary, A.; Wolverton, C. A general-purpose machine learning framework for predicting properties of inorganic materials. *npj Comput. Mater.* **2016,** *2*, 16028.
(33) Dong, Y.; Wu, C.; Zhang, C.; Liu, Y.; Cheng, J.; Lin, J. Bandgap prediction by deep learning in configurationally hybridized graphene and boron nitride. *npj Comput. Mater.* **2019,** *5*, 26.
(34) Oliynyk, A. O.; Adutwum, L. A.; Rudyk, B. W.; Pisavadia, H.; Lotfi, S.; Hlukhyy, V.; Harynuk, J. J.; Mar, A.; Brgoch, J. Disentangling Structural Confusion through Machine Learning: Structure Prediction and Polymorphism of Equiatomic Ternary Phases ABC. *J. Am. Chem. Soc.* **2017,** *139*, 17870-17881.
(35) Xie, Y.; Zhang, C.; Hu, X.; Zhang, C.; Kelley, S. P.; Atwood, J. L.; Lin, J. Machine Learning Assisted Synthesis of Metal–Organic Nanocapsules. *J. Am. Chem. Soc.* **2020,** *142*, 1475-1481.
(36) Granda, J. M.; Donina, L.; Dragone, V.; Long, D.-L.; Cronin, L. Controlling an organic synthesis robot with machine learning to search for new reactivity. *Nature* **2018,** *559*, 377-381.
(37) Ahneman, D. T.; Estrada, J. G.; Lin, S.; Dreher, S. D.; Doyle, A. G. Predicting reaction performance in C–N cross-coupling using machine learning. *Science* **2018,** *360*, 186-190.
(38) Porwol, L.; Kowalski, D. J.; Henson, A.; Long, D. L.; Bell, N. L.; Cronin, L. An autonomous chemical robot discovers the rules of inorganic coordination chemistry without prior knowledge. *Angew. Chem. Int. Ed.* **2020,** *59*, 11256-11261.
(39) Coley, C. W.; Thomas, D. A.; Lummiss, J. A. M.; Jaworski, J. N.; Breen, C. P.; Schultz, V.; Hart, T.; Fishman, J. S.; Rogers, L.; Gao, H.; Hicklin, R. W.; Plehiers, P. P.; Byington, J.; Piotti, J. S.; Green, W. H.; Hart, A. J.; Jamison, T. F.; Jensen, K. F. A robotic platform for flow synthesis of organic compounds informed by AI planning. *Science* **2019,** *365*, eaax1566.
(40) Epps, R. W.; Bowen, M. S.; Volk, A. A.; Abdel-Latif, K.; Han, S.; Reyes, K. G.; Amassian, A.; Abolhasani, M. Artificial Chemist: An Autonomous Quantum Dot Synthesis Bot. *Adv. Mater.* **2020,** *32*, 2001626.
(41) Burger, B.; Maffettone, P. M.; Gusev, V. V.; Aitchison, C. M.; Bai, Y.; Wang, X.; Li, X.; Alston, B. M.; Li, B.; Clowes, R.; Rankin, N.; Harris, B.; Sprick, R. S.; Cooper, A. I. A mobile robotic chemist. *Nature* **2020,** *583*, 237-241.
(42) Coley, C. W.; Eyke, N. S.; Jensen, K. F. Autonomous Discovery in the Chemical Sciences Part I: Progress. *Angew. Chem. Int. Ed.* **2020,** *59*, 22858-22893.
(43) Coley, C. W.; Eyke, N. S.; Jensen, K. F. Autonomous Discovery in the Chemical Sciences Part II: Outlook. *Angew. Chem. Int. Ed.* **2020,** *59*, 23414-23436.
(44) Tabor, D. P.; Roch, L. M.; Saikin, S. K.; Kreisbeck, C.; Sheberla, D.; Montoya, J. H.; Dwaraknath, S.; Aykol, M.; Ortiz, C.; Tribukait, H.; Amador-Bedolla, C.; Brabec, C. J.; Maruyama, B.; Persson, K. A.; Aspuru-Guzik, A. Accelerating the discovery of materials for clean energy in the era of smart automation. *Nat. Rev. Mater.* **2018,** *3*, 5-20.
(45) Eyke, N. S.; Koscher, B. A.; Jensen, K. F. Toward Machine Learning-Enhanced High-Throughput Experimentation. *Trend. Chem.* **2021,** *3*, 120-132.
(46) Flores-Leonar, M. M.; Mejía-Mendoza, L. M.; Aguilar-Granda, A.; Sanchez-Lengeling, B.; Tribukait, H.; Amador-Bedolla, C.; Aspuru-Guzik, A. Materials Acceleration Platforms: On the way to autonomous experimentation. *Curr. Opin. Green Sustain. Chem.* **2020,** *25*, 100370.

(47) Nikolaev, P.; Hooper, D.; Webber, F.; Rao, R.; Decker, K.; Krein, M.; Poleski, J.; Barto, R.; Maruyama, B. Autonomy in materials research: a case study in carbon nanotube growth. *npj Comput. Mater.* **2016,** *2*, 16031.
(48) Xie, Y.; Zhang, C.; Su, J.-W.; Deng, H.; Zhang, C.; Lin, J. Rapid Synthesis of Zeolitic Imidazole Frameworks in Laser-Induced Graphene Microreactors. *ChemSusChem* **2019,** *12*, 473-479.
(49) Parrilla-Gutierrez, J. M.; Sharma, A.; Tsuda, S.; Cooper, G. J. T.; Aragon-Camarasa, G.; Donkers, K.; Cronin, L. A programmable chemical computer with memory and pattern recognition. *Nat. Commun.* **2020,** *11*, 1442.
(50) Lin, J.; Peng, Z.; Liu, Y.; Ruiz-Zepeda, F.; Ye, R.; Samuel, E. L. G.; Yacaman, M. J.; Yakobson, B. I.; Tour, J. M. Laser-induced porous graphene films from commercial polymers. *Nat. Commun.* **2014,** *5*, 5714.
(51) Wahab, H.; Jain, V.; Tyrrell, A. S.; Seas, M. A.; Kotthoff, L.; Johnson, P. A. Machine-learning-assisted fabrication: Bayesian optimization of laser-induced graphene patterning using in-situ Raman analysis. *Carbon* **2020,** *167*, 609-619.
(52) Henson, A. B.; Gromski, P. S.; Cronin, L. Designing Algorithms To Aid Discovery by Chemical Robots. *ACS Cent. Sci.* **2018,** *4*, 793-804.
(53) Le, T. C.; Winkler, D. A. Discovery and Optimization of Materials Using Evolutionary Approaches. *Chem. Rev.* **2016,** *116*, 6107-6132.
(54) Xue, D.; Balachandran, P. V.; Hogden, J.; Theiler, J.; Xue, D.; Lookman, T. Accelerated search for materials with targeted properties by adaptive design. *Nat. Commun.* **2016,** *7*, 11241.
(55) Yuan, R.; Liu, Z.; Balachandran, P. V.; Xue, D.; Zhou, Y.; Ding, X.; Sun, J.; Xue, D.; Lookman, T. Accelerated Discovery of Large Electrostrains in $BaTiO_3$-Based Piezoelectrics Using Active Learning. *Adv. Mater.* **2018,** *30*, 1702884.
(56) Holzwarth, U.; Gibson, N. The Scherrer equation versus the 'Debye-Scherrer equation'. *Nat. Nanotechnol.* **2011,** *6*, 534-534.
(57) Mekki-Berrada, F.; Ren, Z.; Huang, T.; Wong, W. K.; Zheng, F.; Xie, J.; Tian, I. P. S.; Jayavelu, S.; Mahfoud, Z.; Bash, D.; Hippalgaonkar, K.; Khan, S.; Buonassisi, T.; Li, Q.; Wang, X. Two-step machine learning enables optimized nanoparticle synthesis. *npj Comput. Mater.* **2021,** *7*, 55.
(58) Wang, Z.-L.; Ogawa, T.; Adachi, Y. Influence of Algorithm Parameters of Bayesian Optimization, Genetic Algorithm, and Particle Swarm Optimization on Their Optimization Performance. *Adv. Theory Simul.* **2019,** *2*, 1900110.